

Article

Wind Tunnel Experiments on Parallel Blade–Vortex Interaction with Static and Oscillating Airfoil

Andrea Colli * , Alex Zanotti  and Giuseppe Gibertini

Dipartimento di Scienze e Tecnologie Aerospaziali, Politecnico di Milano, Via La Masa 34, 20156 Milan, Italy; alex.zanotti@polimi.it (A.Z.); giuseppe.gibertini@polimi.it (G.G.)

* Correspondence: andrea.colli@polimi.it

Abstract: This study aims to experimentally investigate the effects of parallel blade–vortex interaction (BVI) on the aerodynamic performances of an airfoil, in particular as a possible cause of blade stall, since similar effects have been observed in literature in the case of perpendicular BVI. A wind tunnel test campaign was conducted reproducing parallel BVI on a NACA 23012 blade model at a Reynolds number of 300,000. The vortex was generated by impulsively pitching a second airfoil model, placed upstream. Measurements of the aerodynamic loads acting on the blade were performed by means of unsteady Kulite pressure transducers, while particle image velocimetry (PIV) techniques were employed to study the flow field over the blade model. After a first phase of vortex characterisation, different test cases were investigated with the blade model both kept fixed at different incidences and oscillating sinusoidally in pitch, with the latter case, a novelty in available research on parallel BVI, representing the pitching motion of a helicopter main rotor blade. The results show that parallel BVI produces a thickening of the boundary layer and can induce local flow separation at incidences close to the stall condition of the airfoil. The aerodynamic loads, both lift and drag, suffer important impulsive variations, in agreement with literature on BVI, the effects of which are extended in time. In the case of the oscillating airfoil, BVI introduces hysteresis cycles in the loads, which are generally reduced. In conclusion, parallel BVI can have a detrimental impact on the aerodynamic performances of the blade and even cause flow separation, which, while not being as catastrophic as in the case of dynamic stall, has relatively long-lasting effects.



Citation: Colli, A.; Zanotti, A.; Gibertini, G. Wind Tunnel Experiments on Parallel Blade–Vortex Interaction with Static and Oscillating Airfoil. *Fluids* **2024**, *9*, 111. <https://doi.org/10.3390/fluids9050111>

Academic Editors: Guangjian Zhang and Stéphane Le Dizès

Received: 28 March 2024

Revised: 28 April 2024

Accepted: 7 May 2024

Published: 10 May 2024



Copyright: © 2024 by the authors. Licensee MDPI, Basel, Switzerland. This article is an open access article distributed under the terms and conditions of the Creative Commons Attribution (CC BY) license (<https://creativecommons.org/licenses/by/4.0/>).

Keywords: blade–vortex interaction; BVI; fluid–structure interaction; rotorcraft; wind tunnel; PIV; oscillating airfoil

1. Introduction

Blade–vortex interaction (BVI), which can broadly be defined as the interaction between a rotor blade and a coherent vortical structure, is an unsteady phenomenon characteristic of the complex aerodynamic environment of rotary-wing aircraft [1]. While many of the early works regarded helicopter flight—and in particular, powered descent with the main rotor essentially passing through its own wake—as the main example of BVI occurrence, nowadays, the range of interest has greatly increased given the wide variety of vehicle configurations featuring multiple rotors, from tilt-rotors to compound helicopters, drones, micro aerial vehicles (MAVs), and multi-copter configurations typical of electric vertical take-off and landing (eVTOL) machines. Part of this interest in BVI has classically been associated with its relevance concerning noise production [2,3] (e.g., blade slap sound), but in the literature, the effect of the interaction on the blade aerodynamic loads, in terms of unsteady impulsive variations, often very significant, has always been recognised [4].

Typically, different typologies of BVI are identified based on the relative orientation between the impacting vortex and the blade, resulting in three main categories: parallel BVI, perpendicular BVI, and normal (i.e., out-of-plane) BVI, each with its own peculiar behaviour. An overview of the associated phenomena can be found in [5]. Naturally, in a

real-case rotor environment, any interaction will generally be a combination of the three; nonetheless, this subdivision is useful for a more fundamental study of the behaviour of BVI.

In recent times, particular attention has been brought to the topic of perpendicular BVI, as several studies, both experimental and numerical [6–9], on oscillating blades reported that an interaction of this kind can be the triggering source of dynamic stall of the blade, with a significant detrimental effect on the performances of the airfoil. On the other hand, the research on parallel BVI has mostly been limited to static airfoil models, and highlighted issues with flow separation only in the case of an airfoil at a very high incidence [10–13]; studies of vortex interaction with oscillating bodies have been focused on leading edge impingement or on the behaviour of periodic vortex patterns [5], rather than on the loads generated.

In the last few years, moreover, research in parallel BVI has been performed also outside of the field of rotary-wing aerodynamics, for example, investigating the improvement effect of streamwise vortices on airfoil efficiency [14] or, concerning parallel BVI, studying the interaction of an airfoil or wing with a vortical gust. In the latter case, the literature includes high-fidelity CFD simulations [15,16] and wind tunnel experiments [17,18], albeit at low Reynolds number, and reports on the impulsive changes in the aerodynamic loads during BVI. In particular, the work by [15] studied the viscous effects associated with the vortex–airfoil interaction, showing boundary layer instability and separation.

The aim of the present study is to assess the behaviour of parallel BVI in terms of the influence on the airfoil aerodynamic performances, with a particular focus on macroscopic features of flow separation and stall, to investigate whether effects similar to those observed for perpendicular BVI can occur. By considering a static airfoil at different incidences, the dependence on the blade loading of the BVI effects can be characterised. Finally, the interaction is also tested on a periodically oscillating blade, the study of which extends the literature on the topic of parallel BVI and is of key importance to the application to helicopter aerodynamics.

For these purposes, an experimental test rig was developed for the generation of a suitable vortex and the following study of its interaction with an airfoil model, and an extensive wind tunnel test campaign was conducted including both unsteady pressure measurements to evaluate the loads on the blade and two-dimensional, two-component particle image velocimetry (2D-2C PIV) techniques to investigate the flow field resulting from the interaction. For the vortex generation, the strategy of having an impulsively pitched upstream airfoil was employed, which is common in the literature on parallel BVI [19–21]: the generated vortex is essentially the starting vortex which is released at the trailing edge of the airfoil as a consequence of this sharp motion, resulting from the rolling up of the wake; the vortex is then convected downstream by the wind tunnel flow.

This relatively simple, two-dimensional, test case was chosen to focus on the fundamental behaviour of the vortex–airfoil interaction; taking into account the limitations of the available literature to the interaction with low-incidence airfoils, for the present work, relatively high-load conditions were chosen, which could be representative of those encountered by a helicopter rotor retreating blade, particularly susceptible to stall behaviour.

In the following, the experimental setup will be described together with the data analysis and reduction techniques; then, the results of the campaign will be presented and discussed. For the sake of brevity, throughout the text, the generic term “vortex” will be used in place of the appropriated scientific term “vortical structure”, when referring to the main structure generated to produce the interaction.

2. Materials and Methods

The tests were conducted in the “S. De Ponte” subsonic wind tunnel at Politecnico di Milano, a closed-loop wind tunnel with a 1 by 1.6 m test chamber, a maximum speed of 55 m/s, and a maximum turbulence level of 0.1%.

As previously mentioned, the setup consisted of two airfoil models in a tandem configuration, with one (the vortex generator) placed upstream of the other (the blade model) in the wind tunnel test chamber, as shown in Figure 1.



Figure 1. Schematic view (a) and picture (b) of the test rig assembly in the wind tunnel; in the latter, the blade model is visible in the foreground, while the vortex generator is in the background.

The blade model is a pre-existing aluminum machined assembly composed of two lateral sections and a narrower middle section, attached to an internal metallic frame of four airfoil ribs connected by three wing boxes. Two different middle sections can be interchanged: a plain one, and one with a series of holes spanning the section chord, on both the upper and lower surfaces, to be used as taps for pressure measurements. The model chord is $c = 0.3$ m with a uniform span-wise distribution, while the span is $b = 0.9$ m. The NACA 23012 airfoil section was used, as is typical of helicopter blades. Tubular shafts, connected to the ribs at each extremity in correspondence of the quarter-chord axis, allow the model to be mounted on self-aligning bearings and pivoted around that axis. More details on the blade model characteristics, including locations of the pressure taps and structural analysis, are available in [22].

The blade model is placed horizontally in the wind tunnel test section by means of an external supporting structure of aluminum profiles. In order to control the rotation of the model around the pitch axis, a Parker SME115 brushless electrical motor (Parker Hannifin Corp., Cleveland, OH, USA) is connected to one of the shafts through a double-cardanic steel laminae coupling, to account for angular and axial displacements, and through a 12:1 planetary gear. The control of the pitching motion was exploited to easily set the geometrical incidence of the model during the static interaction study, and then employed to realise the oscillating motion of the model.

The vortex generator model is composed of a steel spar, with a square section of 3 cm side, around which a carbon fibre skin was laminated. To allow for the presence of the spar, a custom airfoil section shape was employed, joining the leading edge portion of a NACA 0018 to the trailing edge section of a NACA 0016, with the spar in the quarter-chord position. A styrofoam filler was shaped accordingly and used as a reference for the lamination process. The resulting model has a chord $c_g = 0.2$ m and a span $b_g = 0.9$ m. An assembly of tubular shafts, bearings, laminae coupling, and supporting structure, similar to that used for the blade model, allows one to mount the vortex generator in the wind tunnel test section, 1.2 m upstream of the blade model quarter-chord axis; the vertical position was manually adjustable by sliding the support braces along vertical struts. The vortex generator is attached on one end to a Parker SME170 brushless electrical motor (Parker Hannifin Corp., Cleveland, OH, USA), with a nominal torque of 35 Nm and a peak torque of 100 Nm, which is used to control its pitching motion.

A programmable logic controller (PLC), commanded via a LabView (v. 2018) graphical interface, is used to control both motors. To measure their angular position, the signal from the internal Heidenhain SinCos EnDat absolute encoders (Dr. Johannes Heidenhain GmbH, Traunreut, Germany), with an accuracy of $\pm 400''$, is acquired; any mechanical backlash or

model deformation is neglected in the following study. The initial angular positioning in pitch with respect to the wind tunnel centreline was measured by a digital inclinometer, with an accuracy of 0.01° . The motion of the vortex generator was of fundamental importance: in order for a single, well-defined, concentrated vortex to be released, the pitching motion has to be fast compared to a time scale relative to the free-stream velocity and the generator chord; in particular, the rotation should be completed in a time interval smaller than c_g/V_∞ [20]. This relation poses an upper limit to the free-stream velocity, and therefore to the flow Reynolds number, depending on the speed achievable by the motion system. The amplitude of the rotation was chosen to be of $\Delta\alpha_g = 10^\circ$ and a trial-and-error procedure was conducted to fine-tune the parameters of the motor drive internal PID controller and obtain the fastest possible motion without overshoot or oscillations; the result was a time interval to complete the motion of $\Delta t = 11$ ms. Based on this result, a wind tunnel free-stream velocity of $V_\infty = 15$ m s⁻¹ was selected, in compliance with the aforementioned constraint, corresponding to a Reynolds number of $Re = (cV_\infty)/\nu = 300,000$, relative to the airfoil chord; this value of the Reynolds number is in the range of the ones found in the literature for similar studies [19,20].

The pitching motion of the generator was realised by feeding the PLC a sawtooth-like input signal, with a comparatively slow ramp to set the airfoil at the incidence of $\alpha_g = 0^\circ$ followed by an impulsive rotation to $\alpha_g = 10^\circ$, which causes the release of the vortex. These values were chosen in order to have a high value of lift, and thus circulation, of the vortex generator and to have a counter-clockwise vortex. Both before and after the ramp, i.e., before and after the vortex interaction, a waiting period is added to allow the flow to reach steady conditions. The final input signal has a total period of 2 s. More details on the mechanism of vortex generation can be found in [23].

The same motion of the generator was employed also for the tests with the oscillating blade model, while the latter was pitched according to a sine wave with amplitude 10° given by the law $\alpha = \alpha_0 + 10^\circ \sin 2\pi ft$, where α_0 is the starting airfoil incidence and f is the frequency of the motion; for the former, different values were chosen, ranging from 5° to 7° , to study the differences in BVI as the blade incidence increases, while the latter was chosen as to achieve a reduced frequency $k = \pi fc/V_\infty = 0.1$, resulting in a motion with a period of 0.628 s. These values are typical of “light” dynamic stall tests. The motion of the generator was adjusted in order to have a vortex interaction every three periods of the blade model, i.e., every 1.884 s, while keeping the duration of the impulsive pitching equal to that of the previous static tests so that the two kinds of interactions could be compared. This condition is different from that experienced by a rotor blade in a real-case scenario, where the BVI would occur at each cycle, assuming periodic conditions, but the results showed that the effects of the interaction exhaust themselves well before a full cycle, which leads to the hypothesis that the BVI behaviour would be closely similar in the two cases. Finally, the commanded time histories of the motion of the two models were shifted with respect to each other in order to have the interaction happening at two different positions during the airfoil oscillation, both in the descending portion, one right after the peak incidence is reached (“high incidence interaction”, HII) and one when the airfoil is at an incidence 5° lower than the peak one, approximately (“low incidence interaction” LII); the relative time shift between the HII and LII oscillation time histories is of 30 ms.

Concerning the vortex generator, particular care is needed in taking into account its presence in the wind tunnel in order to correctly interpret the actual test conditions and the subsequent results. As previously mentioned, after the vortex release, the vortex generator is at an incidence of $\alpha_g = 10^\circ$; therefore, its induction on the blade model has to be included in the reference condition (“baseline”) against which to evaluate the effects of the interaction; on the other hand, the conditions before the vortex generation will be different from the baseline: in fact, the process of vortex generation can be interpreted by substituting the generator model with the vortex itself, held fixed in the same position, and then allowed to be convected by the free-stream flow.

2.1. PIV Measurements

The PIV setup is composed of a dual Nd-YAG Evergreen laser (LUMIBIRD SA, Lannion, France), with an energy of 200 mJ per pulse, and two ILA sCMOS cameras (ILA_5150 GmbH, Aachen, Germany), with a resolution of 2560×2160 pixel. The laser was placed below the floor of the wind tunnel test section, in which a mid-span optic window allowed the light to illuminate the flow; because of this positioning, the blade model was installed with the suction side facing the floor when $\alpha = 0^\circ$. Oil droplets, with diameter in the range of 1–2 μm , generated by a Laskin-nozzle particle generator, were employed as tracer particles. An ILA synchroniser (ILA_5150 GmbH, Aachen, Germany) was used to control the acquisition timing, managing the laser and the cameras; an Hall-effect sensor was mounted on one of the vortex generator support shafts, and its signal, corresponding to $\alpha_g = 0^\circ$, was used as a trigger. The PIV images were processed with a multi-pass method over a 32×32 pixel grid, with no previous filtering but with outlier detection and interpolation, and finally phase-averaged; the PIVTEC PIVview2C [24] software (v. 3.9) was used for the task. Considering a 0.2 px sub-pixel interpolation accuracy [25], the error on the velocity field can be estimated to be below 2% of the free-stream velocity.

A first phase of PIV measurement was conducted in order to characterise the generated vortex velocity profile; for this phase, the blade model was not installed in the wind tunnel.

Secondly, the blade model was inserted, and its vertical position was adjusted in such a way that the vortex would impinge approximately at the leading edge of the airfoil, with an upward trajectory going over the suction side. This procedure was executed for a geometrical incidence of the blade model of 14° and was not repeated for different angles as it was seen that the change in position due to the rotation was offset by the change in circulation around the airfoil, resulting in a similar vortex relative trajectory over a range of incidences 10° – 16° .

For the study of the interaction, PIV measurements were taken at different time instants by adding a time delay to the triggering signal; a range of times starting from the vortex approaching the blade model leading edge and up to the vortex having travelled downstream of the trailing edge was considered. Measurements with no vortex interaction were also performed, with the vortex generator fixed at $\alpha_g = 0^\circ$ and 10° ; in those cases, the acquisition sequence was manually triggered.

2.2. Pressure Measurements

For the pressure measurement phase, the mid-span section of the blade model was swapped with the appropriate one, instrumented with 21 pressure taps distributed chord-wise in the middle of the section; details on the positions of the taps can be found in [22]. The taps were fitted with nylon pipes in which Kulite XCS-093-2D (Kulite Semiconductor Products, Inc., Leonia, NJ, USA) unsteady pressure transducers were inserted, with sealing rubber O-rings; the combined non-linearity, hysteresis, and repeatability error is indicated to be typically within 0.1% of the full scale output. The signals from the transducers were acquired by a NI cDAQ-9172 with NI 9237 bridge modules (National Instruments Corporation, Austin, TX, USA) at a sampling rate of 10 kHz; simultaneously, the angular positions of the vortex generator and of the blade model were acquired by a NI 9215 module (National Instruments Corporation, Austin, TX, USA) on the same cDAQ. It is to be noticed that during the test campaign, five transducers suffered a failure, which therefore reduced the number of available data points.

The pressure measurements during the vortex interaction study were acquired for 20 s, starting from the same trigger signal used for the PIV acquisition. Given the periodicity of the motion, 10 cycles were included in this period; each acquisition was repeated 10 times, for a total of 100 cycles of vortex generation and interaction acquired for each test condition; the time histories were finally phase-averaged, and a moving average filter with a ten-point kernel was applied to reduce noise. Measurements with no vortex interaction were also acquired at different incidences in order to characterise the airfoil polar, with the vortex

generator fixed at $\alpha_g = 0^\circ$ and 10° ; in those cases, the acquisition sequence was manually triggered and the data were time-averaged and filtered to obtain the steady values.

The data from the pressure measurements were postprocessed by a custom Python (v. 3.10) script, performing the computation of the pressure coefficient and the integration to obtain the lift and drag acting on the blade model; in particular, the airfoil section was divided into straight panels, over which the pressure was obtained from the values measured at the taps through linear interpolation based on the curvilinear abscissa. The lift C_l and drag C_d coefficients were then computed as

$$C_l = \frac{L}{\frac{1}{2}\rho V_\infty^2 c} \quad C_d = \frac{D}{\frac{1}{2}\rho V_\infty^2 c}, \quad (1)$$

where L and D are, respectively, the lift and drag per unit span obtained by the integration of the pressure data and ρ is the air density. Finally, the two-dimensional boundary corrections from [26] were applied to the data, in particular concerning wake blockage and solid blockage, especially relevant for the higher incidences tested. It is to be noticed that no attempt was made to extend these corrections to the trajectory of the vortex itself, that is, to determine the influence of the test being conducted in the wind tunnel rather than in free air on the convection and evolution of the vortex.

In the case of the unsteady measurements during vortex interaction, the processing method was applied to the time history of the pressure distribution, obtaining the corresponding time histories of the aerodynamic coefficients. The same corrective factors computed for the stationary case were used for the whole time history.

The same procedure was also applied to the analysis of the data recorded from the interaction on the oscillating airfoil; in this case, however, no corrective factors were applied. Measurements were taken of the oscillating airfoil with no vortex interaction to serve as the baseline reference.

3. Results and Discussion

In the analysis of the following results, a reference frame placed at the quarter-chord point of the blade model and aligned with the free-stream velocity is employed, as shown in Figure 2.

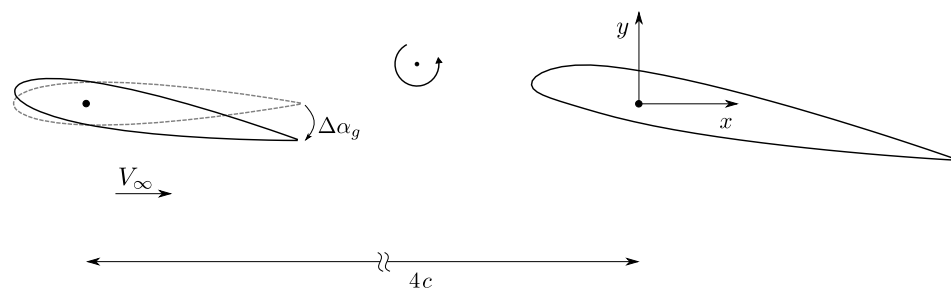


Figure 2. Schematics of the setup and reference frame employed. The vortex generator is on the left, and the blade model on the right.

The non-dimensional time $\tau = tV_\infty/c$ is also introduced, where t is the time in seconds and $t = 0$ is chosen as the instant at which the impulsive motion of the vortex generator ends. One time unit, therefore, corresponds to the time it takes for the vortex, assumed to be convected by the free-stream velocity, to travel over the blade model chord.

3.1. Vortex Characterisation

The averaged PIV measurements of the isolated vortex (Figure 3) show that the vortex core, defined as the flow region delimited by the local extrema in the velocity profile, presents a circular shape, with a radius of $r_{core}/c = 0.0328$. The circulation, computed by integrating along the core perimeter, is $\Gamma/(cV_\infty) = 0.066$, corresponding to a vortex

Reynolds number $Re_\Gamma = \Gamma/\nu = \Gamma/(cV_\infty)Re = 19,800$. By comparing with literature data from experiments on tip vortices released by helicopter rotor models [27], the size of the present vortex fits very well in the typical range for tip vortices, while its core circulation is consistent with newly released vortices. Concerning the vortex Reynolds number, which is related to turbulent diffusion and vortex growth rate [28], the present value falls within the range of measurements for model-scale rotors [29]. The induced tangential velocity u_θ profile is also reported in Figure 3 and compared to a Vatisstas model [30]:

$$u_\theta = \frac{r}{(1 + r^{2n})^{1/n}}, \tag{2}$$

where r is the distance from the vortex centre, normalised to have a core size of $r = 1$; it can be seen that a close fit to the experimental data is obtained by setting $n = 1$.

To characterise the dispersion associated with vortex meandering and the repeatability of the generation process, a statistics analysis over all the PIV image couples was performed by considering each couple separately and identifying the vortex centre position through the λ_2 criterion [31]: the results showed that the data from the averaged PIV measurements overestimate the vortex size by less than 1%, with respect to the size determined by statistical analysis on the separate image couples. Therefore, no specific procedure was adopted to align the position of the vortex across all the images prior to the averaging process; such a procedure, moreover, would not have been applicable to the following measurements with the blade model.

In conclusion, the vortex generation process was deemed suitable for the parallel BVI study, being able to reliably produce an isolated, coherent vortex with adequate size and strength.

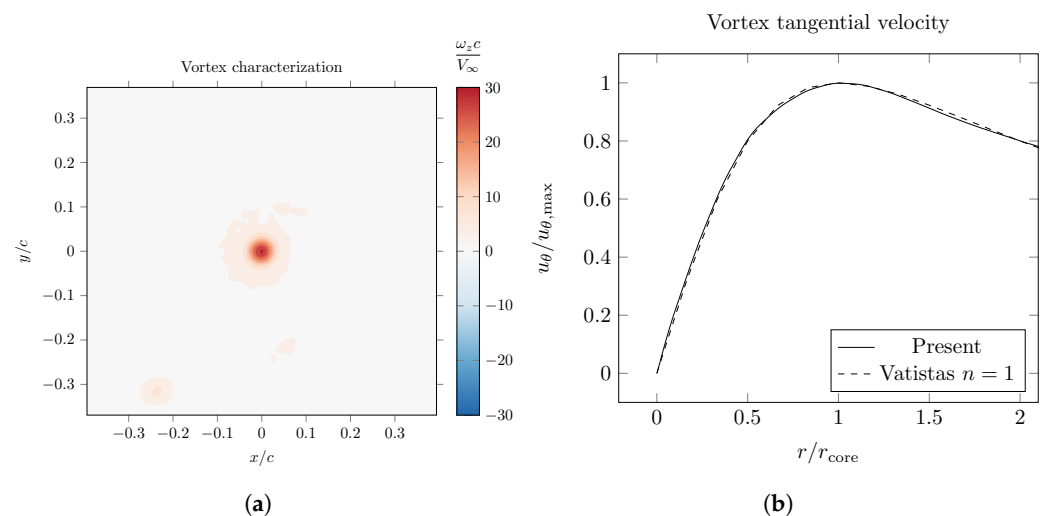


Figure 3. Vorticity contour (a) and tangential velocity u_θ profile (b) for the averaged vortex, from PIV measurements.

3.2. Airfoil Polar

The aerodynamic coefficients computed from the pressure measurements on the stationary airfoil (Figure 4), considering the case with $\alpha_g = 0^\circ$, show a behaviour of the lift curve that is consistent with the literature work on NACA 23012 at a similarly low Reynolds number [32–34]. In particular, the maximum lift coefficient has a value of 1.163, which is found in correspondence of $\alpha = 14.6^\circ$. It is to be noticed that no evident laminar separation bubble, which is a common feature in airfoils of this type, was visible from the experimental data; while this might be ascribed to the relatively low number of pressure taps in the relevant portion of the airfoil, it could also hint to three-dimensional flow behaviour influencing boundary layer transition and separation. Wind tunnel data from [35] also show a limited presence, if any, of a laminar separation bubble, which could

confirm a sensibility of the phenomenon to experimental conditions. The lift curve in the condition with $\alpha_g = 10^\circ$, i.e., the baseline condition, shows a less abrupt stall behaviour with a slightly lower maximum lift coefficient of 1.133 for $\alpha = 15.6^\circ$; this increase in the stall geometric incidence is expected due to the effect of the upstream vortex generator, which decreases the effective incidence of the blade model by about 1° . During the tests, a hysteresis of the stall behaviour was observed. It should be noticed that the reported drag values include only pressure drag, being obtained from the pressure measurements.

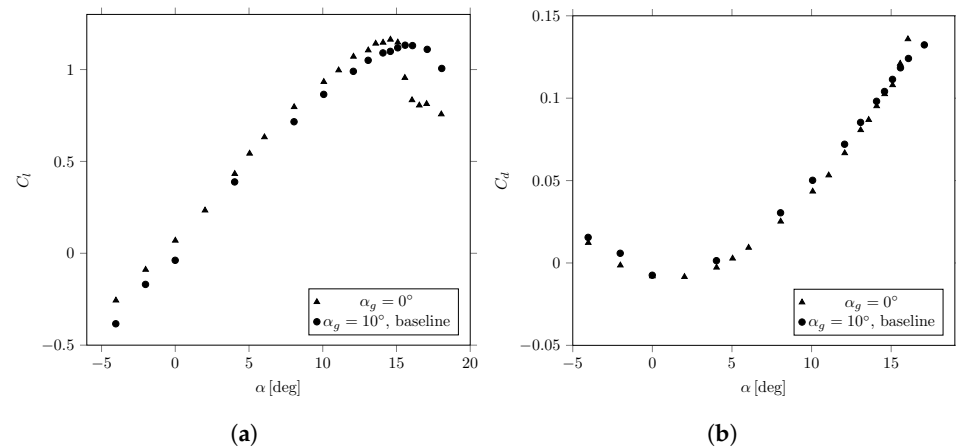


Figure 4. Lift (a) and drag (b) coefficients from integration of pressure measurements for the baseline condition $\alpha_g = 10^\circ$ and for $\alpha_g = 0^\circ$.

3.3. Vortex Interaction—Static Airfoil

The measurements of the interaction between the vortex and the blade model show the vortex approaching with a trajectory impinging on the leading edge of the airfoil, and then moving towards the suction side and along it. During the interaction, the vortex remains coherent, with a core region which is clearly identifiable, although distorted into a more oval shape; the dimensions of the core also increase slightly.

In Figure 5 the sequence of the interaction with the airfoil at incidence $\alpha = 14^\circ$ shows how the main effect of the vortex passage is a very noticeable thickening of the boundary layer along the suction side of the airfoil, as indicated by the vorticity contours. At first, the thickening is more severe at the chord-wise positions corresponding to and immediately downstream of the vortex position, while it reduces drastically immediately upstream: this behaviour is expected given the counter-clockwise rotation of the vortex, as the induced velocity field tends to displace the flow away from the airfoil surface ahead of the vortex, and towards the surface behind it. Once at approximately the mid-chord position, the upstream edge of the increased thickness region appears to lag behind the vortex, while its downstream edge continues to correspond to the vortex position: this results in the widening of the region and, at later times, in the formation of two almost separate “bubbles” of increased vorticity; in this region, moreover, the vorticity has opposite sign to that of the airfoil and is comparable in magnitude. As the vortex gets closer to the trailing edge, a portion of recirculating flow can be identified as associated with the vorticity bubble. This viscous behaviour is consistent with the observations by [36] and the analysis of [37,38], concerning the vortex interaction with a wall: these authors report the formation of a similar vorticity bubble and indicate its cause in the adverse pressure gradient produced by the presence of the vortex, which induces a suction peak beneath the core. The fact that no “eruption” of this bubble can be seen may be attributed to the different flow conditions of the present case, with an airfoil at incidence, with respect to a plane wall.

Similarities can also be found with the results of the LES computations of [15], which report thickening of the boundary layer, with laminar separation and the formation of a counter-rotating vortical disturbance. While detailed comparisons are difficult to make,

given the lower incidence of the airfoil and the much larger interacting vortex that they used in the work, the mechanism of flow separation presently observed is likely to be similar.

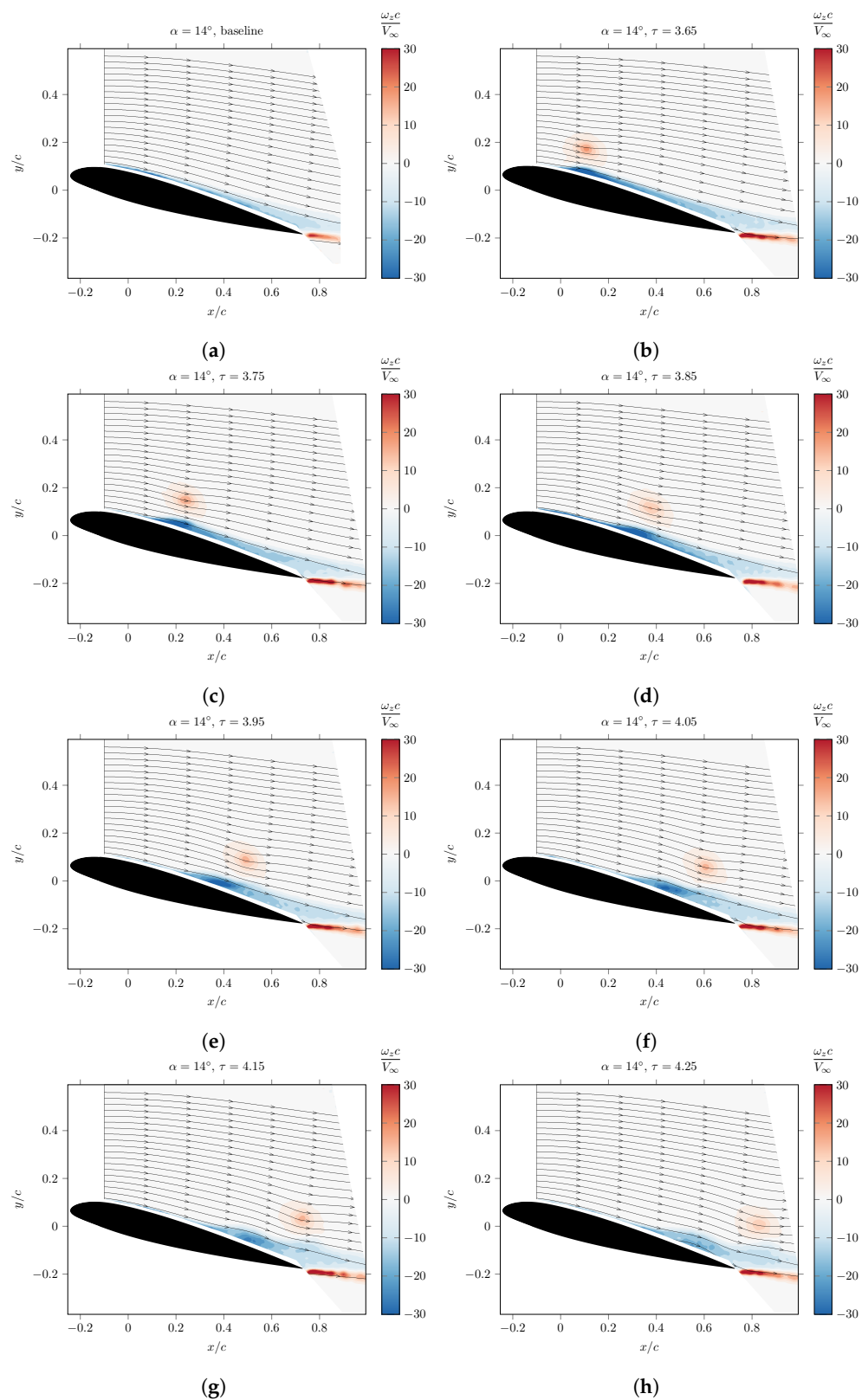


Figure 5. Vorticity contours from PIV measurements of the flow field during the vortex interaction with the static airfoil at 14° and comparison with baseline: (a) baseline, (b) $\tau = 3.65$, (c) $\tau = 3.75$, (d) $\tau = 3.85$, (e) $\tau = 3.95$, (f) $\tau = 4.05$, (g) $\tau = 4.15$, (h) $\tau = 4.25$.

The description just presented can be applied to the behaviour of the interaction with the airfoil at $\alpha = 15^\circ$, as shown in Figure 6, with the main differences being that in the latter case, the thickness increase does not reduce downstream, thus not forming a bubble as definite as in the former case; and that recirculating flow regions are clearly visible, starting from earlier interaction times. In particular, the boundary layer is more severely displaced and the separated region extends from around 50% of the chord, persisting well after the vortex has passed the trailing edge of the blade. This behaviour could be expected given that the incidence is closer to the stall condition and the boundary layer would be more prone to separating under disturbances. While the appearance of separated flow regions, both for $\alpha = 14^\circ$ and $\alpha = 15^\circ$, could be explained in terms of the essentially inviscid effect of the vortex induced velocity increasing the effective incidence of the airfoil, viscous effects also play a significant role, as shown by the vorticity distribution in the boundary layer being heavily influenced by the passage of the vortex, with the appearance of secondary structures and their subsequent evolution.

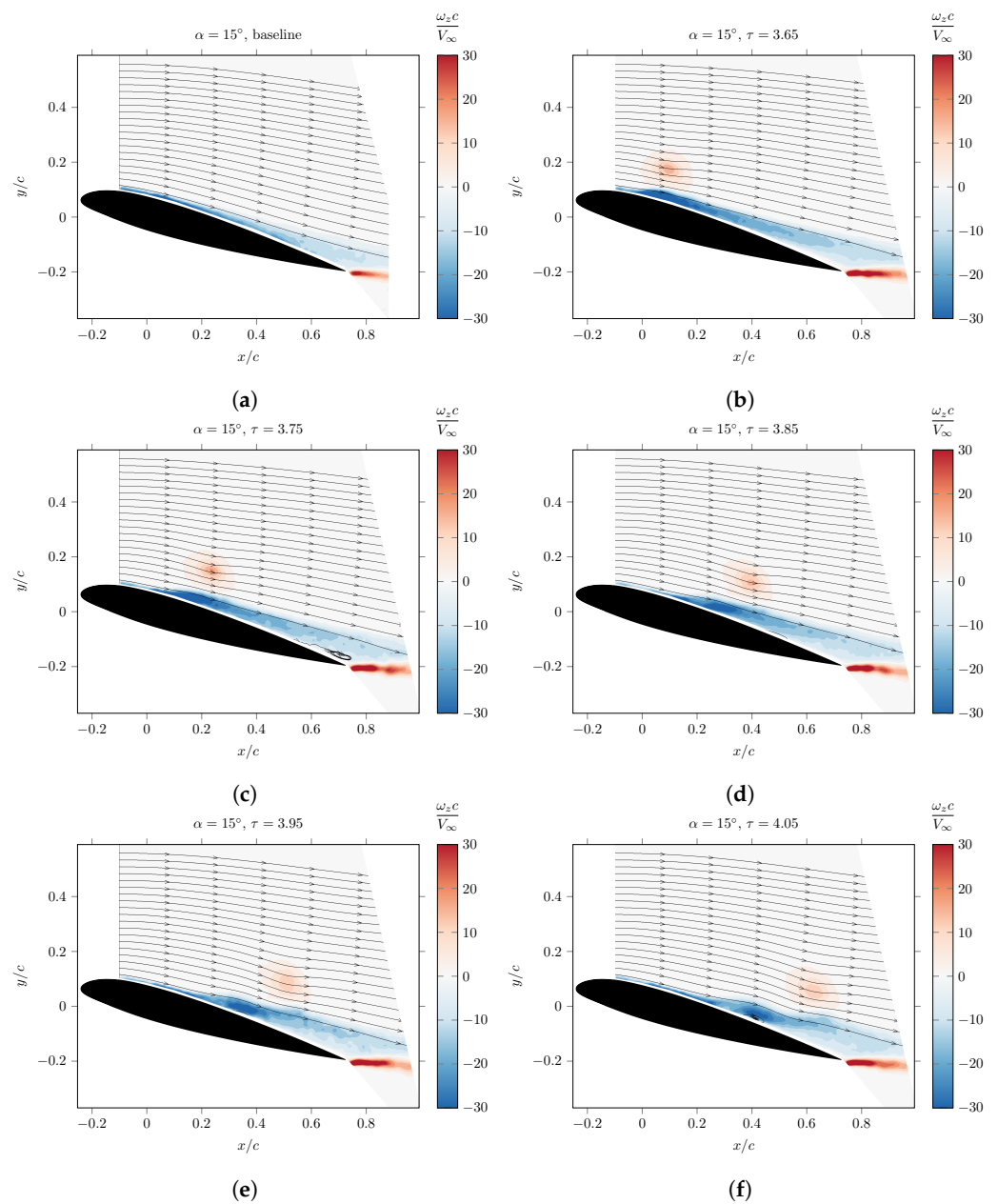


Figure 6. Cont.

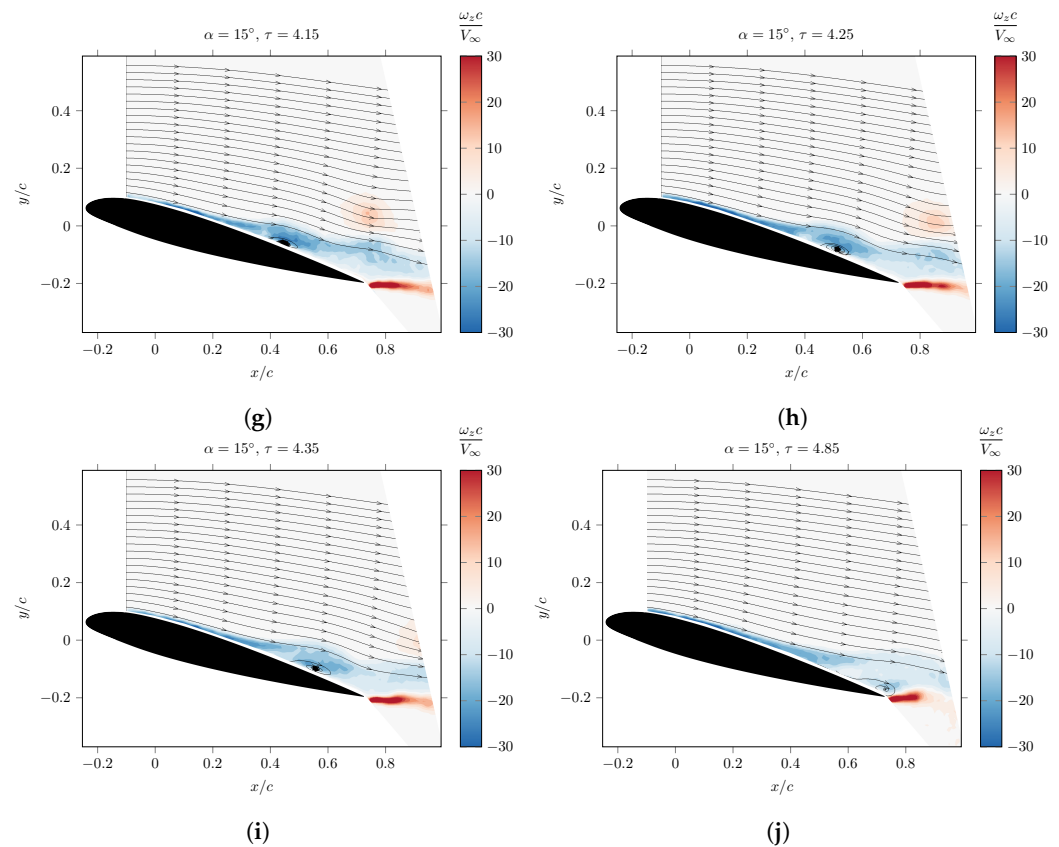


Figure 6. Vorticity contours from PIV measurements of the flow field during the vortex interaction with the static airfoil at 15° and comparison with baseline: (a) baseline, (b) $\tau = 3.65$, (c) $\tau = 3.75$, (d) $\tau = 3.85$, (e) $\tau = 3.95$, (f) $\tau = 4.05$, (g) $\tau = 4.15$, (h) $\tau = 4.25$, (i) $\tau = 4.35$, (j) $\tau = 4.85$.

The measurements of the interaction in the case with the airfoil at $\alpha = 10^\circ$, presented in Figure 7, show that the above reasoning can still be applied, but the effect of the vortex is much reduced, with the vorticity bubble being smaller and more localised, and no separation of the flow being evident.

From the PIV measurements, therefore, it can be concluded that the interaction produces a thickening of the airfoil boundary layer, with the development of a vorticity bubble; this effect is local, limited to a region which moves downstream approximately following the vortex chordwise position. The magnitude of this effect, both in terms of the increase in thickness and the size of the affected region, is greater for the higher incidences of the airfoil, particularly for those close to the stall condition. The transiency of the observed phenomenon—that is, the fact that upstream of the vortex, the flow field tends to return to the undisturbed conditions—is to be expected by the nature of the interaction, as explained above. In conclusion, trailing-edge stall-like separation is observed as a result of the parallel blade–vortex interaction for high incidences of the airfoil, close to the maximum lift conditions. This is consistent with the interpretation of the effect of the vortex as inducing an increase in incidence, given also the comparatively smooth stall behaviour observed from the airfoil polar. This reasoning, however, is too simplistic since the behaviour cannot be reduced to a mere variation of incidence in unperturbed conditions, but the unsteadiness of the phenomenon must be taken into account. By projecting the results shown here, moreover, it could be argued that a vortex of higher circulation could disrupt more severely the boundary layer downstream of it in such a way that even the restoring influence of the upstream induced velocity is not able to reattach the flow, which would produce a separated condition all over the airfoil chord. This hypothesis could not be tested with the present test rig, as the strength of the vortex is limited by the pitching motion of the vortex generator.

Other works in the literature [10,11,13] presented flow separation as a result of parallel BVI, also in the case of highly loaded airfoil only, already close to the stall conditions. The behaviour of the interaction in those cases, however, differed from the present as it triggered a separation bubble in the leading edge region, which then propagated downstream. This difference could be explained by the overall blade model behaviour, which, as already mentioned, did not feature a definite laminar separation bubble, suggesting a more turbulent flow; three-dimensional effects could also modify the flow conditions.

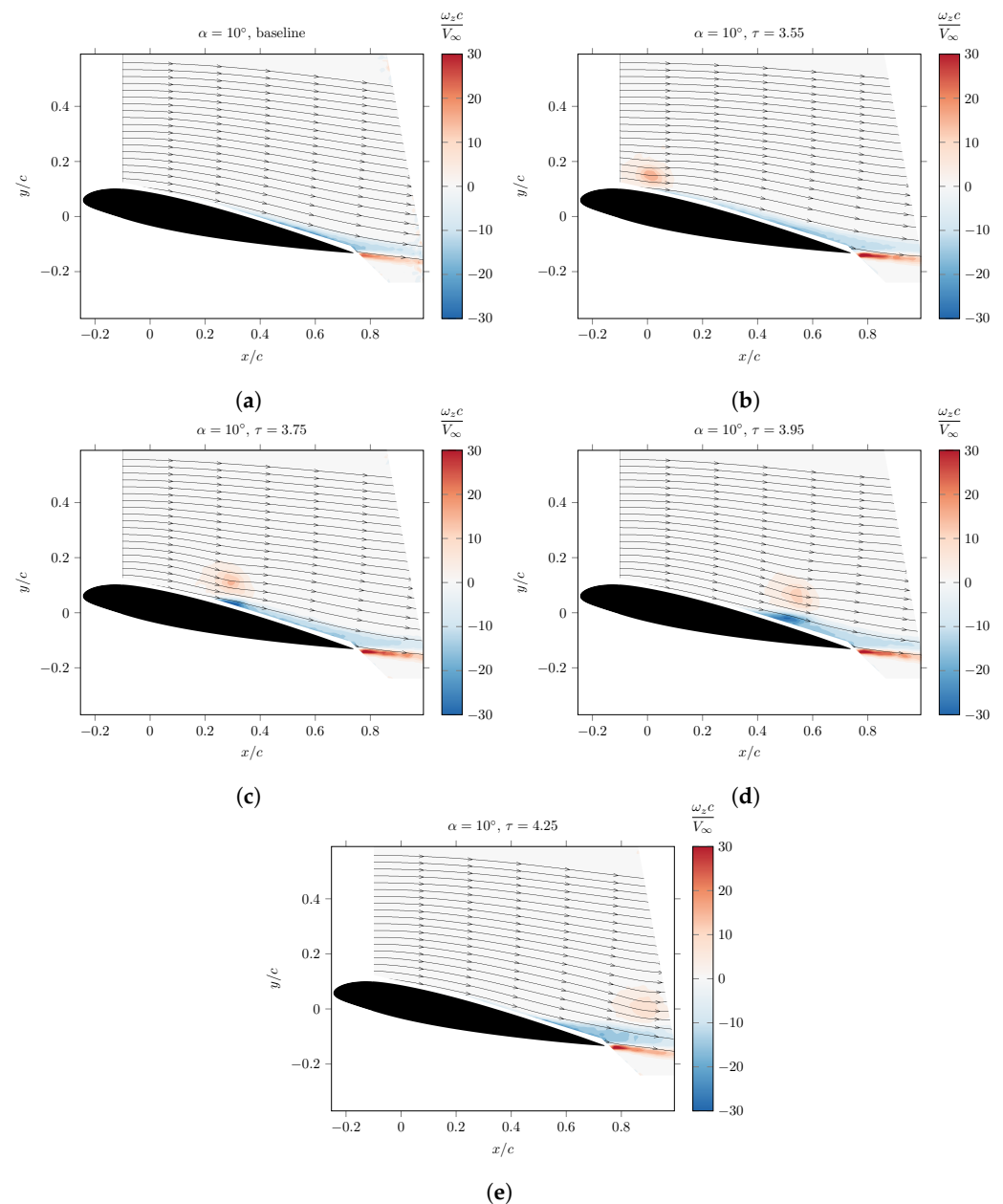


Figure 7. Vorticity contours from PIV measurements of the flow field during the vortex interaction with the static airfoil at 10° and comparison with baseline: (a) baseline, (b) $\tau = 3.55$, (c) $\tau = 3.75$, (d) $\tau = 3.95$, (e) $\tau = 4.25$.

More insight on the effects of the interaction can be gained from the time histories of the aerodynamic coefficient computed from the pressure measurements. To better show this, the variation ΔC_l in the lift coefficient is introduced as

$$\Delta C_l = \frac{C_l - \bar{C}_l}{\bar{C}_l}, \tag{3}$$

where \bar{C}_l is the lift coefficient in the baseline condition; the same reasoning leads to the definition of the variation in the drag coefficient ΔC_d . Of course, the above definitions are meaningful only where $\bar{C}_l \gg 0$ (and similarly for the \bar{C}_d), which is always the case in the proximity of the maximum vortex interaction, as shown below.

Concerning the lift coefficient C_l during the blade–vortex interaction, as seen in Figure 8 and from Table 1, a substantial impulsive increase is evident for all the incidences. This effect is consistent with the behaviour of BVI as described in the literature, and it is usually explained in terms of the induced upwash of the approaching vortex, followed by a corresponding downwash effect, as already mentioned above. Comparison with the PIV measurements shows that the peak in the lift coefficient is found in correspondence with the vortex reaching the leading edge portion of the airfoil, which is also in accord with the findings of similar works [10,20]. The time τ_{peak} of the peak occurrence is also very similar for all three incidences, with the slight differences accounting for the variations in position of the airfoil and in induced flow. The lift increase is inversely proportional to the blade incidence, with the highest variation being +38% for $\alpha = 10^\circ$. This effect can be expected as the vortex strength is the same for all three cases, while the magnitude of the induced velocity field of the airfoil increases with its incidence, so that the influence of the vortex, in terms of its induced velocity, is proportionally smaller.

Immediately after the peak, the lift falls briskly to values below the baseline: it can be noticed that this difference with respect to the baseline is greater for $\alpha = 15^\circ$, which reaches $\Delta C_l = -14.2\%$, while it is similar, although smaller in magnitude, for the two other cases. This trend, which contrasts with the interpretation given above for the lift peak, can be explained by the occurrence of flow separation as observed from the PIV measurements, which differentiates the behaviour at the highest incidence.

The return to the baseline \bar{C}_l values, for all cases, is noticeably slower than the sharp peak, taking several time units before reaching a steady state; it can also be noticed how in the case of $\alpha = 15^\circ$, the lift coefficient remains very slightly higher than its baseline value. This persistence of the disturbance following the interaction could be attributed to the relatively slow evolution and eventual disappearance of the secondary vortical structures in the boundary layer of the airfoil. To compute an estimate of this settling time, the following approach was chosen: firstly, the difference ΔC_l between the lift measured during the interaction and its baseline value is computed for all times; then, starting from the time instant corresponding to the peak induced by the interaction, the settling time $\Delta\tau$ is determined as the time interval after which the maximum variation in ΔC_l keeps under 2% of the maximum value of the baseline C_l :

$$\Delta\tau = \tau_{2\%} - \tau_{\text{peak}}, \tag{4}$$

where $\tau_{2\%}$ is the time value such that

$$\frac{\max \Delta C_l - \min \Delta C_l}{\max \bar{C}_l} < 2\% \tag{5}$$

for all $\tau > \tau_{2\%}$, up to a suitably large time. This strategy allows for a comparison of the settling times between the static airfoil interactions and the following oscillating airfoil interactions, while also accounting for any discrepancies between the steady state and the baseline values.

The computed settling times for the static airfoil interaction cases are reported in the last column of Table 1. The largest value of $\Delta\tau$ is found in correspondence of $\alpha = 10^\circ$, which might reflect the greater perturbing effect induced by the interaction at this lower incidence. The difference between the settling times in the other two cases can be accounted for by considering the larger flow separation occurring for $\alpha = 15^\circ$. Despite the different behaviours among the three cases, as shown by the PIV measurements, the values of $\Delta\tau$ are relatively similar and the time histories show a comparable trend.

Concerning the drag coefficient C_d , a greater variation in the magnitude of the behaviour can be seen among the three cases. In particular, in the case $\alpha = 10^\circ$ the interaction has the first effect of reducing the drag value, with a downward peak which exactly corresponds in time to the lift peak, representing the same impulsive variation typical of BVI. Drag falls significantly, to almost $\Delta C_d = -60\%$. This behaviour can be explained as a suction effect of the low-pressure field associated to the vortex approaching the leading edge of the airfoil. After this peak, the value of C_d rises sharply with a quick succession of two peaks at around $\Delta C_d = +16.5\%$, before returning to the baseline value. This trend is qualitatively similar in the other two cases: at first the drag is reduced, more briskly, but to a lesser extent with respect to the previous case, which again indicates the greater relative influence of the interaction at low incidences. Then, the drag rises abruptly in a much more significant way: in particular, for $\alpha = 15^\circ$, the variation is as high as $\Delta C_l = +34\%$. This increase in drag, and its dependence on the incidence, can be associated with the occurrence of separated flow, as also indicated by the PIV measurements, as well as with the suction effect mentioned above. It is to be noticed that the appearance of two definite peaks can be attributed to the relative coarse chord-wise spacing between the pressure taps, which causes a loss of spatial resolution when dealing with a very localised phenomenon such as the vortex passage. Nonetheless, it is interesting to point out that the second peak occurs at around $\tau = 4.25$, that is, after the vortex has passed the trailing edge: the load variation can therefore be attributed to the downstream convection of the vorticity bubble or, in general, to secondary structures generated by the vortex interaction.

In conclusion, by examining the pressure data, the effect of the parallel BVI is confirmed as impulsive variations in the aerodynamic loads, with drag being particularly affected. A comparison of the aerodynamic loads time history during the interaction can be made with the results by [15] for the case of the higher relative encounter between vortex and airfoil: the results, for both lift and drag, are in good agreement, at least qualitatively, while a quantitative comparison is difficult to make, given the differences in the test conditions already mentioned above. From their analysis, moreover, secondary spikes in the loads are found to be associated with the vortical structures generated in the boundary layer because of the BVI, which supports the observations made earlier.

Table 1. Vortex interaction with static airfoil at incidence α : minimum and maximum lift ΔC_l and drag ΔC_d variation, time of lift peak occurrence τ_{peak} and settling time $\Delta\tau$.

α [deg]	ΔC_l [%]		ΔC_d [%]		τ_{peak}	$\Delta\tau$
10	-10.3	+38.0	-59.2	+16.5	3.18	9.33
14	-10.6	+29.0	-26.9	+22.0	3.17	7.19
15	-14.2	+27.1	-25.3	+34.3	3.20	8.23

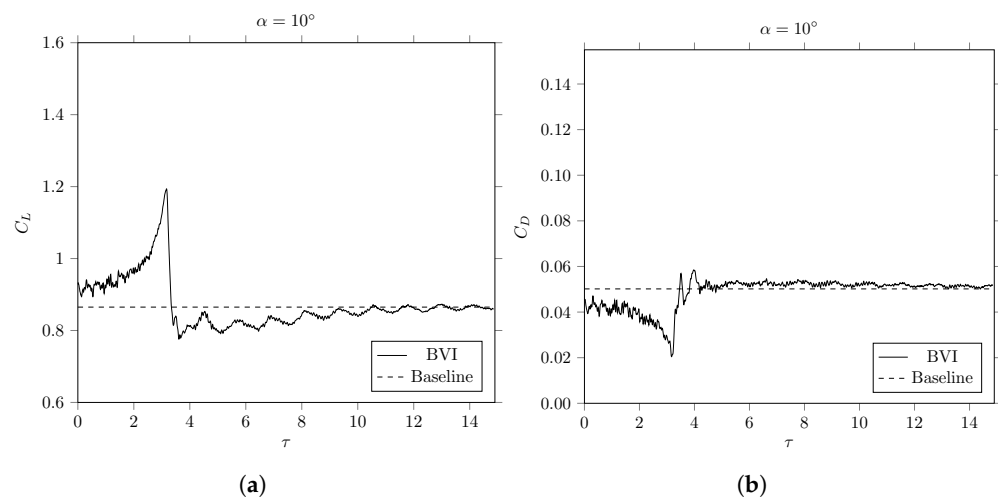


Figure 8. Cont.

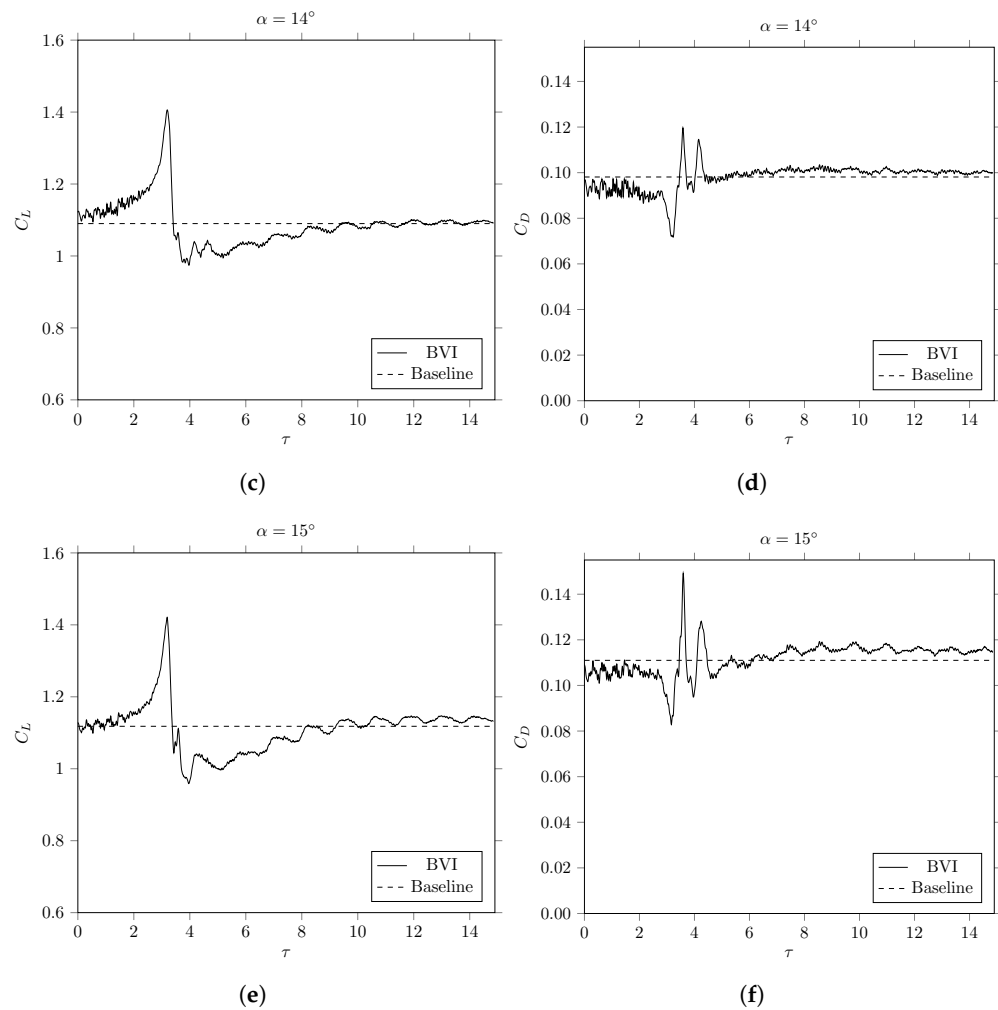


Figure 8. C_l (left) and C_d (right) time histories during the vortex interaction with the static airfoil at different incidences: (a,b) $\alpha = 10^\circ$, (c,d) $\alpha = 14^\circ$, (e,f) $\alpha = 15^\circ$.

3.4. Vortex Interaction—Oscillating Airfoil

From a qualitative point of view, the flow behaviour during the interaction with the oscillating airfoil shows a similarity with the interaction in the case of the static airfoil discussed above. Figures 9–11 present the results from the PIV measurements of the HII cases, showing the thickening of the boundary layer, resulting from the passage of the vortex, with respect to the baseline conditions. A region of separated flow near the trailing edge can be identified, especially for $\alpha_0 = 7^\circ$, but its extent does not appear to be significantly different when compared to the static airfoil cases at the corresponding incidences α ; in particular, there is no indication of large separations or other phenomena related to dynamic stall.

Similar remarks can be made for the LII cases, of which Figure 12 shows the one with $\alpha_0 = 7^\circ$: the perturbation induced by the vortex appears to be less significant than the corresponding HII case at the same α_0 , which is consistent with the fact that the interaction is occurring at a lower incidence, although, at the same time, by comparing with the static case at $\alpha = 10^\circ$ a slightly larger trailing edge separation can be seen.

The results of the unsteady pressure measurements during the interaction with the oscillating airfoil are reported in Figures 13 and 14 in terms of lift coefficient values as a function of blade model incidence. It can be noticed how the data show a small hysteresis cycle for all baseline cases tested (dashed lines in figure); moreover, the fact that a gap is visible in the BVI graph is to be attributed to the different position of the vortex generator during the blade model oscillation cycle, as discussed above.

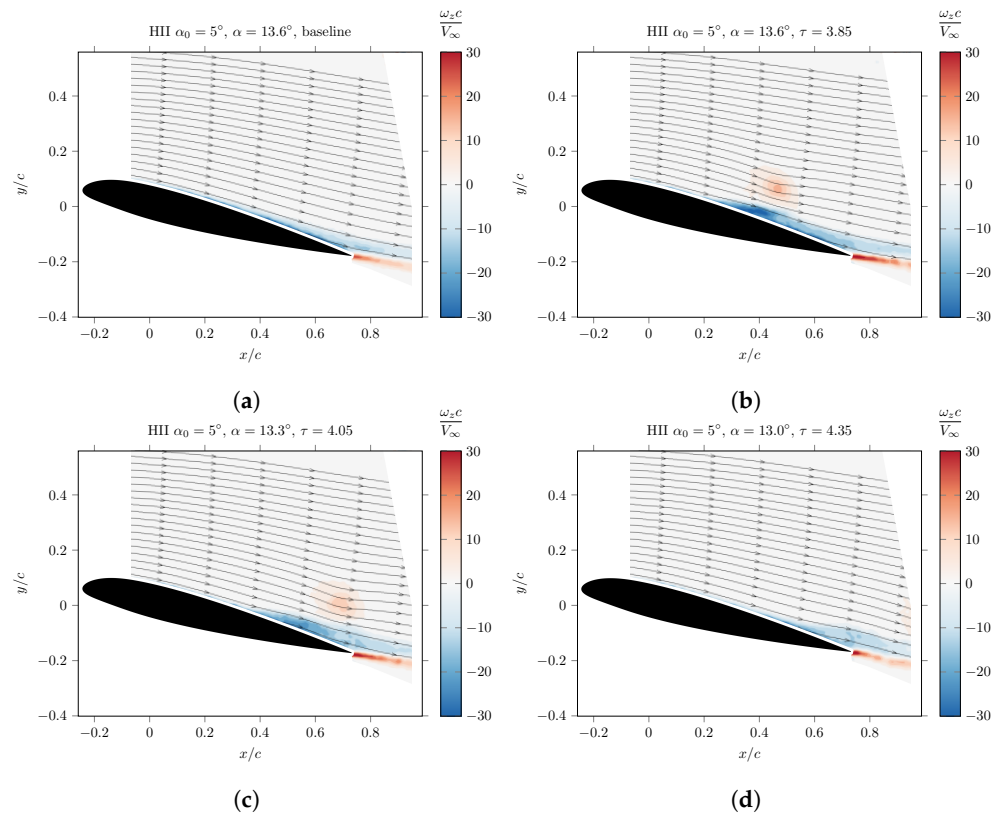


Figure 9. PIV measurements of the flow field during the HII vortex interaction with the oscillating airfoil at $\alpha_0 = 5^\circ$ and comparison with baseline. The actual airfoil incidence α is reported for each time τ : (a) baseline, (b) $\tau = 3.85$, (c) $\tau = 4.05$, (d) $\tau = 4.35$.

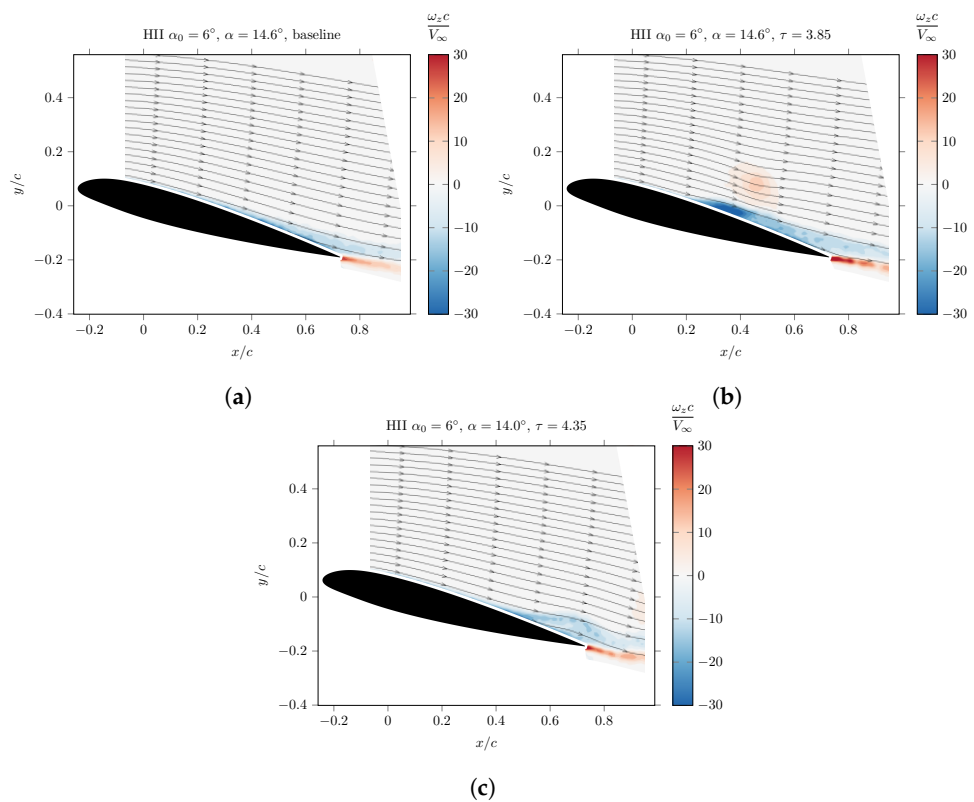


Figure 10. Vorticity contours from PIV measurements of the flow field during the HII vortex interaction with the oscillating airfoil at $\alpha_0 = 6^\circ$ and comparison with baseline. The actual airfoil incidence α is reported for each time τ : (a) baseline, (b) $\tau = 3.85$, (c) $\tau = 4.35$.

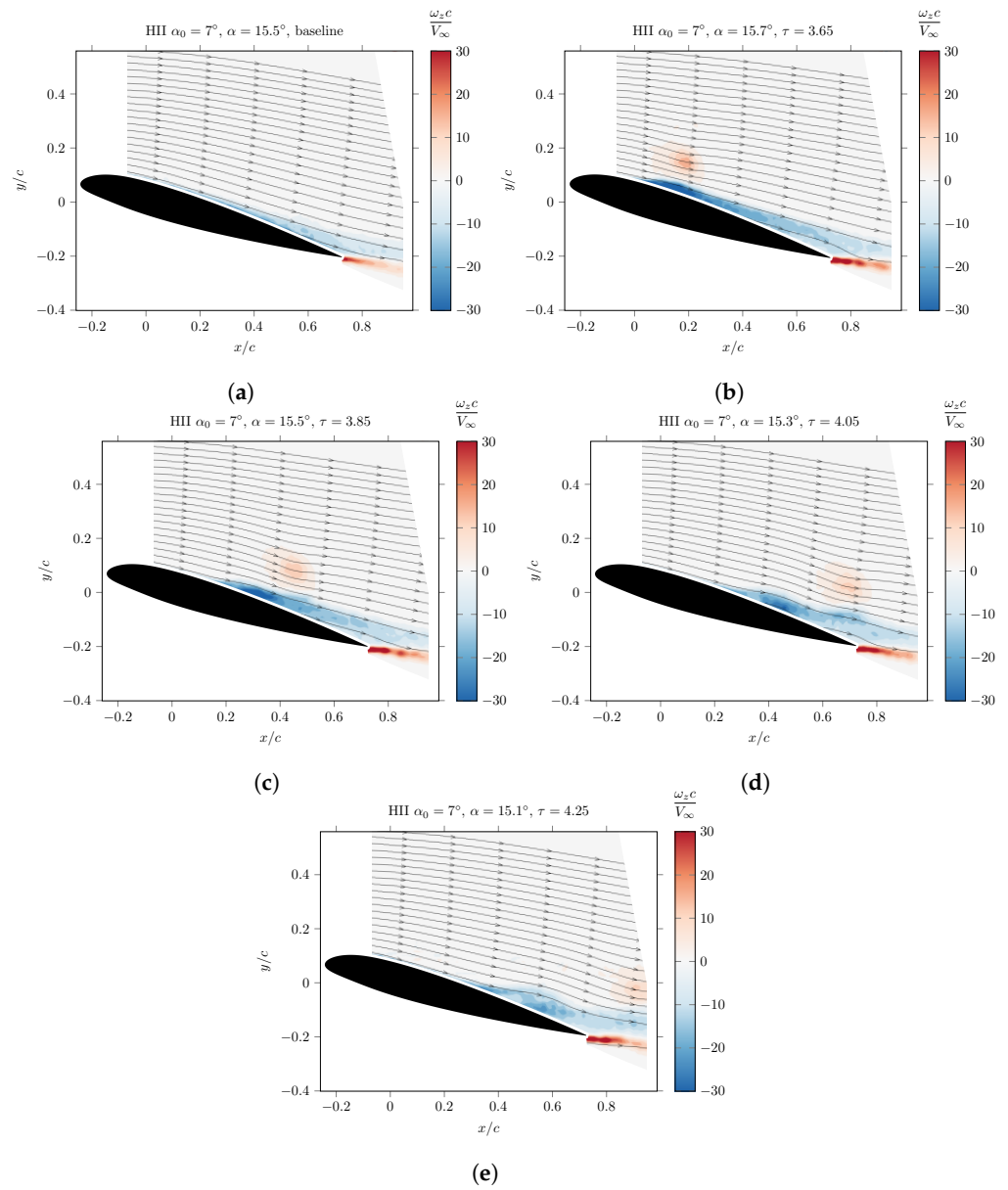


Figure 11. Vorticity contours from PIV measurements of the flow field during the HII vortex interaction with the oscillating airfoil at $\alpha_0 = 7^\circ$ and comparison with baseline. The actual airfoil incidence α is reported for each time τ : (a) baseline, (b) $\tau = 3.65$, (c) $\tau = 3.85$, (d) $\tau = 4.05$, (e) $\tau = 4.25$.

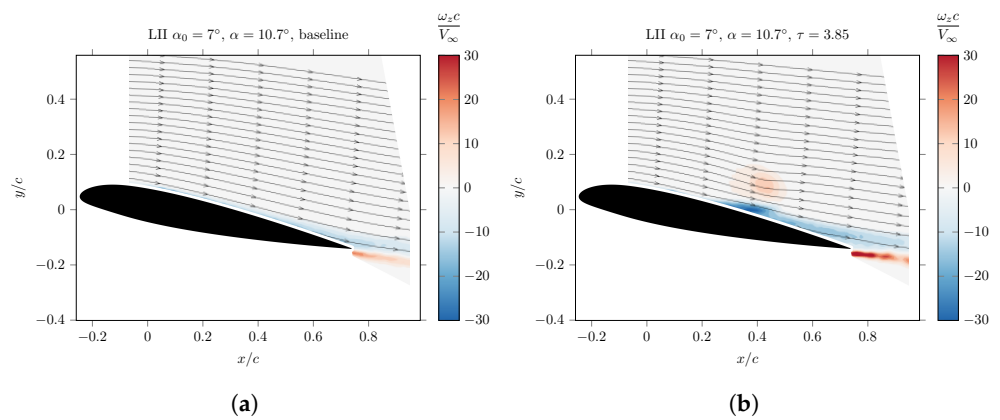


Figure 12. Cont.

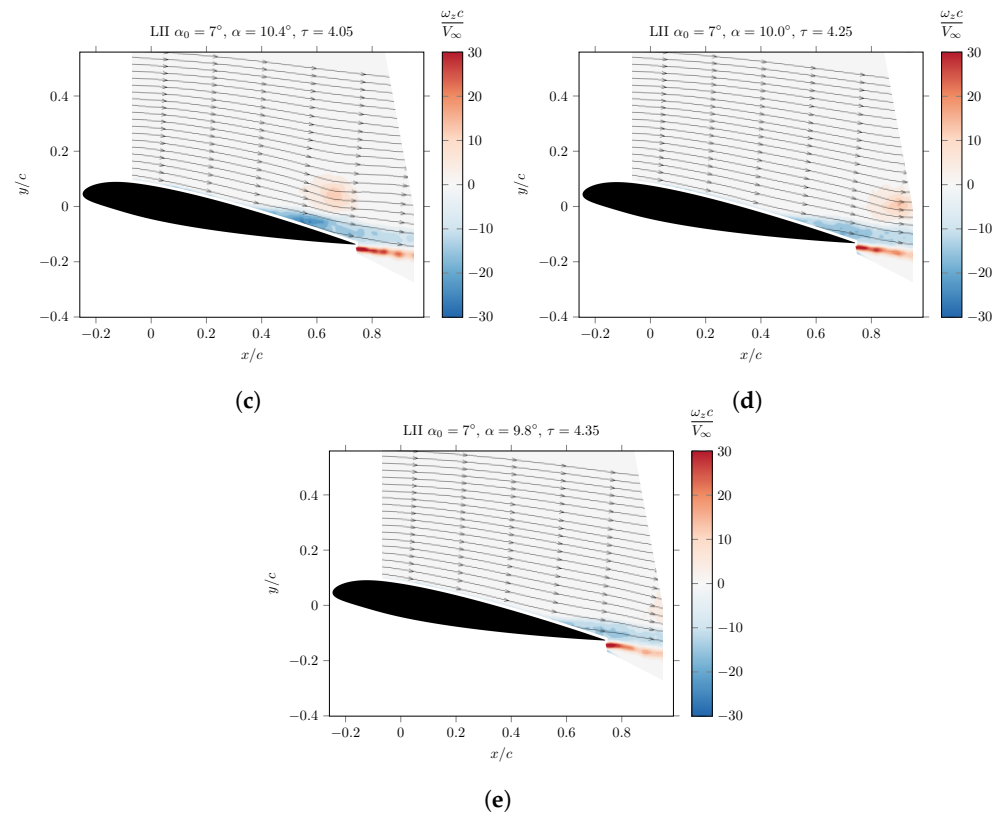


Figure 12. Vorticity contours from PIV measurements of the flow field during the LII vortex interaction with the oscillating airfoil at $\alpha_0 = 7^\circ$ and comparison with baseline. The actual airfoil incidence α is reported for each time τ : (a) baseline, (b) $\tau = 3.85$, (c) $\tau = 4.05$, (d) $\tau = 4.25$, (e) $\tau = 4.35$.

By looking at the measurements for the HII, a sharp peak in C_l can be seen, as expected, followed by an interval where the lift is lower than the baseline values, effectively widening the hysteresis cycle in correspondence of the downstroke motion. This effect is similar to, although not as severe as, dynamic stall behaviour, and it is more evident the higher the incidence. Table 2 reports the relative variations in C_l and C_d along with information on the time of occurrence of the lift peak and the settling time. By comparing with the data in Table 1 the same trends are generally found: τ_{peak} is very similar for all three HII cases, and the maximum C_l increase in correspondence of the peak is inversely proportional to the airfoil incidence; the minimum ΔC_l , however, shows a much greater variation at the highest incidences with respect to the static interaction cases, dropping to almost $\Delta C_l = -26\%$ for $\alpha_0 = 7^\circ$, which is also the case exhibiting a larger hysteresis cycle. Concerning the drag values, the decrease in C_d is similar to the static $\alpha = 14^\circ$ and 15° cases, while there is a much more significant increase in drag, reaching $+75.5\%$ for $\alpha_0 = 7^\circ$; this behaviour can be related to the insurgence of flow separation, as the highest values are recorded in correspondence of the vortex passing over the region close to the trailing edge of the airfoil. In terms of the settling time $\Delta\tau$, very little difference is found among the three HII cases; comparing to Table 1, moreover, it can be seen that these cases present a $\Delta\tau$ lower than in the static interactions.

Table 2 also reports the data from the measurements in the LII cases, while the corresponding trends in C_l are shown in Figure 14. Concerning the airfoil lift, the variations for $\alpha_0 = 5^\circ$ and 6° are similar, and slightly larger in magnitude than the previously described cases, which is expected since the interaction is occurring at lower incidences. The case $\alpha_0 = 7^\circ$ shows a much more detrimental effect, which, again, can be tied to the trailing edge flow separation as shown by the PIV measurements. By looking at the C_d variations, it can be seen that a very large drop is recorded for all LII cases, as low as $\Delta C_d = -82.5\%$; while such values are comparable to the ΔC_d for the $\alpha = 10^\circ$ static airfoil case, the following peak is considerably higher than the corresponding case. The settling times are significantly

larger than in the HII cases, also affecting part of the upstroke motion of the blade model; this difference could hint to a possible restoring effect by the down-stroke motion dynamics itself. For both kinds of interaction, however, the trends confirm that the effects of BVI can be considered to have vanished in less than a period of oscillation, justifying the choice of the motion history for the vortex generator.

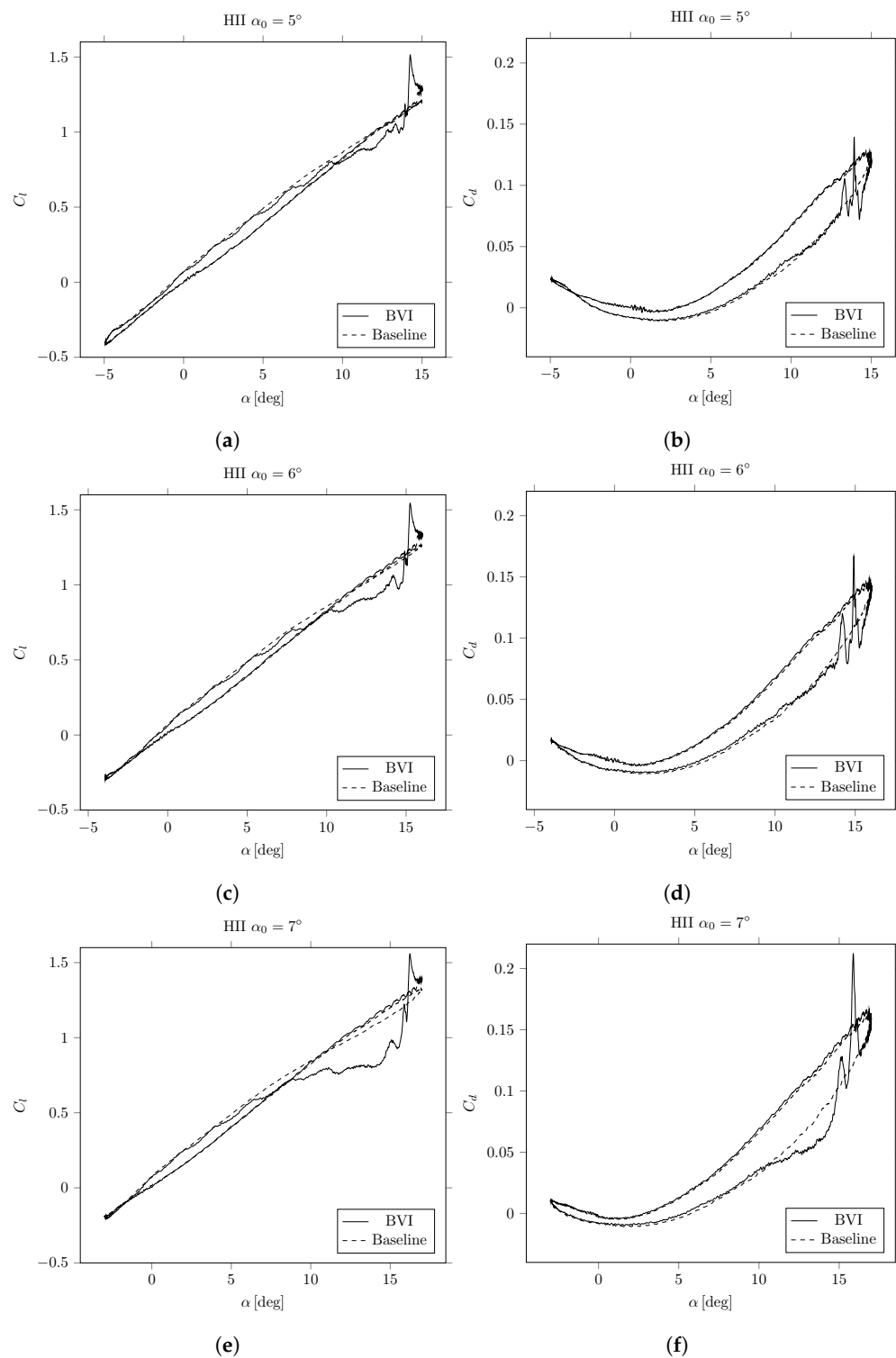


Figure 13. Lift coefficient C_l (left) and drag coefficient C_d (right) as function of blade model incidence α , comparison between HII and baseline for different base incidence α_0 : (a,b) $\alpha_0 = 5^\circ$, (c,d) $\alpha_0 = 6^\circ$, (e,f) $\alpha_0 = 7^\circ$.

By extrapolating the trends described above in the case of the interactions with the static airfoil, it can be suggested that the BVI behaviour is not fundamentally different from that seen in the case of the oscillating blade model when compared at a similar incidence at the moment of interaction. The most noticeable difference, a general increase in drag, can be associated with the insurgence of flow separation at lower incidences than would be the case if the airfoil were static, although the pitching motion seems to affect only weakly the overall effects.

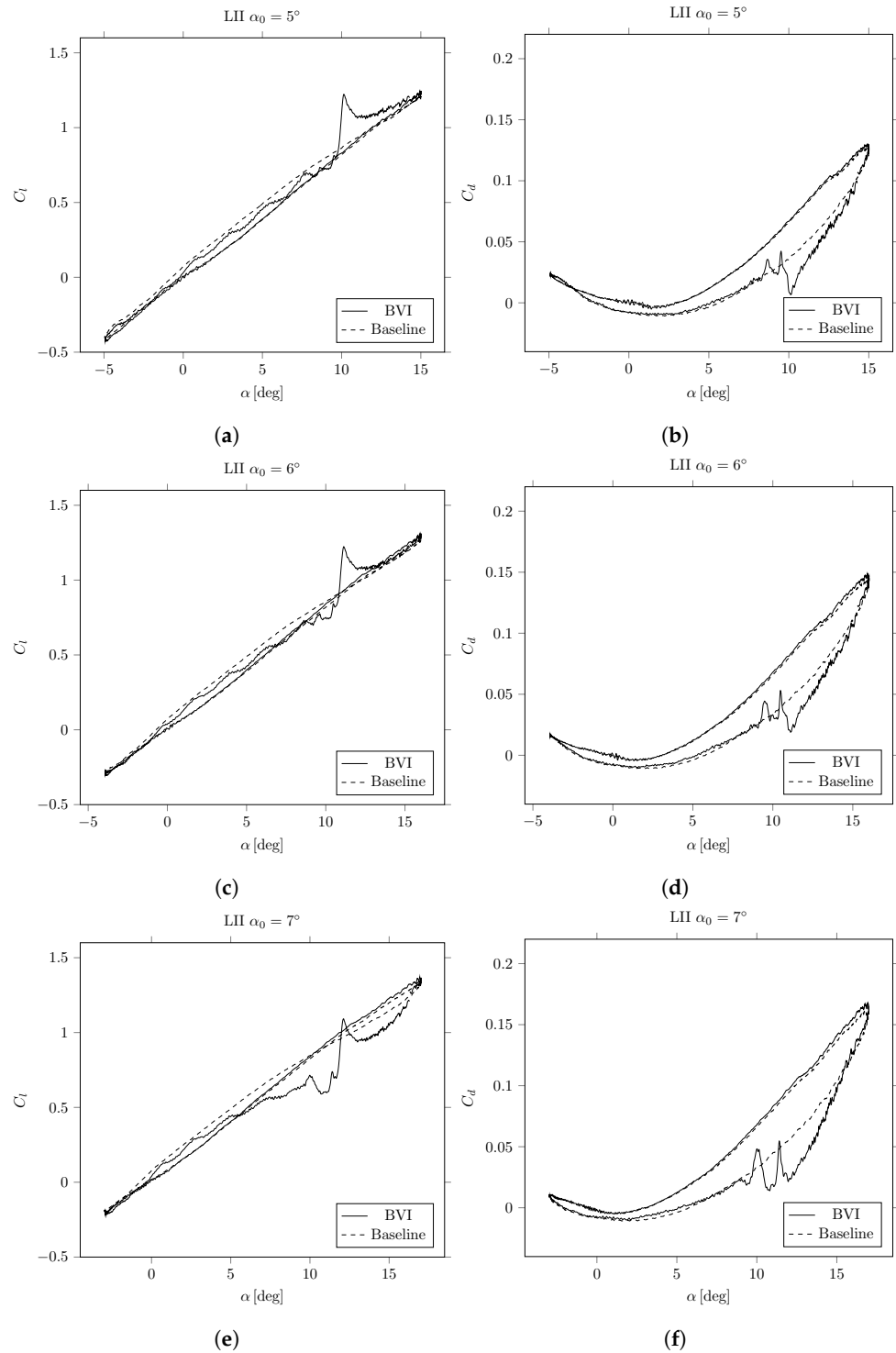


Figure 14. Lift coefficient C_l (left) and drag coefficient C_d (right) as function of blade model incidence α , comparison between LII and baseline for different base incidence α_0 : (a,b) $\alpha_0 = 5^\circ$, (c,d) $\alpha_0 = 6^\circ$, (e,f) $\alpha_0 = 7^\circ$.

Table 2. Vortex interaction with oscillating airfoil with base incidence α_0 : minimum and maximum lift ΔC_l and drag ΔC_d variation, time of lift peak occurrence τ_{peak} and settling time $\Delta\tau$.

Case	α_0 [deg]	ΔC_l [%]		ΔC_d [%]		τ_{peak}	$\Delta\tau$
HII	5	−11.5	+30.3	−29.0	+48.8	3.08	7.45
	6	−15.5	+28.9	−20.9	+53.6	3.08	7.03
	7	−25.9	+26.0	−28.6	+75.5	3.09	7.07
LII	5	−22.5	+39.5	−82.5	+38.9	3.08	10.50
	6	−14.8	+31.9	−59.0	+37.1	3.08	12.51
	7	−34.2	+13.1	−66.3	+47.2	3.09	13.58

4. Conclusions

The aim of this study was to afford an experimental insight into the mechanism of parallel blade–vortex interaction and its effects, in particular in terms of the blade’s overall aerodynamic performance, both in the case of interaction with a static airfoil and in the case of interaction with a sinusoidally pitched airfoil. Unsteady pressure measurements on the blade model were performed, as well as PIV measurements of the flow field in the suction side region of the airfoil. The design of the experimental test rig, with an upstream pitching airfoil model acting as vortex generator, allowed one to obtain a well-developed vortex with the desirable qualities of a reduced size with respect to the blade model and ease and repeatability of the process of generation, which was a key factor for the intensive test campaign.

The results of the measurements concerning the static interaction confirmed the expectations from the literature on the subject, with the blade being subjected to impulsive variation in the aerodynamic loads, which can be related to the upwash and downwash effect of the flow induced by the vortex downstream and upstream of its position, respectively. This unsteady effect is very clearly visible, especially in the comparisons between the baseline values and time history of the lift coefficient, with peaks up to +38%, and of the drag coefficient, which reduces by −59.2% in the most affected case. These variations show a dependence on the blade airfoil incidence, with lower ΔC_l and higher ΔC_d values measured in correspondence with the highest incidences, which can be explained by BVI-induced flow separation and also by considering that the perturbing effect of the vortex would be proportionally lower the higher the incidence. The corresponding PIV data showed a perturbation of the boundary layer over the suction side of the blade airfoil, which thickens as vorticity accumulates in a bubble in correspondence of the passage of the vortex and moves along the suction side following it at a slower speed. For the cases $\alpha = 14^\circ$ and 15° , the vortex passage was seen to trigger trailing-edge flow separation over the aft portion of the airfoil, up to about $0.5c$. Similar flow behaviour is in agreement with the description found in the literature on vortex–airfoil interaction, and vortex–surface interaction in general. Moreover, a significant delay in the return to baseline, undisturbed conditions was recorded, up to $\Delta\tau = 9.33$, which corresponds to several chord lengths after the vortex has passed the blade trailing edge; this could indicate that the unsteady perturbation of the boundary layer dissipates slowly.

The analysis of the interactional behaviour for the case of the oscillating blade model, which represents the main novelty of the present work, showed similarities with the static interaction case. In particular, the variation of the aerodynamic loads with respect to the airfoil incidence presents hysteresis cycles, with a reduction of the lift which affects most of the downstroke phase. This effect is particularly evident for the highest incidence of pitching motion and, for the same incidence, it is greater when the interaction happens as the airfoil downstroke motion has just begun. An increase in the settling time was recorded for the LII cases, with respect to the interaction in the static case. The flow field analysis of the PIV data showed that the BVI behaviour resembles qualitatively the one for the static case, but a region of separated flow can also be seen at low airfoil incidences. In the tested conditions, there was no evidence of dynamic stall behaviour induced by the vortex interaction.

In conclusion, the wind tunnel test campaign confirmed that parallel BVI is an important source of transient aerodynamic loads, which can lead to strong vibrations and impact on the generated noise. From the tested conditions, this kind of interaction does not appear to be able to produce catastrophic flow separation and stall, although, in the case of the oscillating airfoil, a significant hysteresis behaviour with a reduction in the lift coefficient was measured. Ultimately, this behaviour could be explained by the inherent transiency of the parallel interaction, as the potentially detrimental effect of the vortex induced velocity is more limited in time during the interaction, with respect to other conditions such as perpendicular BVI. Nonetheless, the observed effects of the interaction on the airfoil boundary layer and the formation of secondary vortical structures highlight the importance of viscous effects in parallel BVI, which should be taken into account when studying and modelling this kind of interaction.

It is to be noticed that, in the present study, neither the effect of surface roughness nor the influence of vortex strength as a parameter were considered. With respect to the former, no significant variation is expected in the mechanism of the vortex interaction itself, provided that any difference in the stalling behaviour of the airfoil, depending on surface roughness, is taken into account. As to the latter, the strength of the generated vortex was less than ideal for the comparison with BVI in a helicopter rotor environment. It cannot be excluded, therefore, that a stronger vortex could trigger the stall of the blade at low incidences, or induce more severely stalled conditions. The limitation on the strength of the produced vortex is imposed by the current experimental setup, as it depends on the execution time of the impulsive pitching motion of the vortex generator: to overcome it, therefore, the test rig should be updated, e.g., with a more powerful motor, a different vortex generator model, or an altogether different actuation method. Alternatively, a computational approach could be followed, for example, employing high-fidelity LES, which would allow to arbitrarily modify the vortex characteristics and would afford a detailed description of the boundary layer behaviour during the interaction.

Author Contributions: Conceptualisation, A.C., A.Z. and G.G.; methodology, A.C., A.Z. and G.G.; software, A.C.; validation, A.C.; formal analysis, A.C.; investigation, A.C.; resources, A.Z. and G.G.; data curation, A.C.; writing—original draft preparation, A.C.; writing—review and editing, A.Z. and G.G.; visualisation, A.C.; supervision, A.Z. and G.G.; project administration, G.G.; funding acquisition, A.Z. and G.G. All authors have read and agreed to the published version of the manuscript.

Funding: This research received no external funding.

Institutional Review Board Statement: Not applicable.

Data Availability Statement: Dataset available on request from the authors.

Acknowledgments: The authors wish to acknowledge the steadfast support kindly provided by the technical team of the Aerodynamic Laboratory of the Department of Aerospace Science and Technology.

Conflicts of Interest: The authors declare no conflicts of interest.

Abbreviations

The following abbreviations are used in this manuscript:

BVI	Blade–Vortex Interaction
PIV	Particle Image Velocimetry
MAV	Micro Aerial Vehicle
eVTOL	electric Vertical Take-Off and Landing
c	blade model chord
c_g	vortex generator chord
V_∞	wind-tunnel free-stream speed
ρ	air density
ω_z	z-component of the vorticity vector
L	airfoil lift per unit span

D	airfoil drag per unit span
α	blade model incidence
α_g	vortex generator incidence
C_l	airfoil lift coefficient
C_d	airfoil drag coefficient
f	pitch oscillation frequency
k	pitch oscillation reduced frequency
α_0	mean pitch for oscillating airfoil
HII	high-incidence interaction
LII	low-incidence interaction
τ	non-dimensional time
τ_{peak}	time of lift peak
$\Delta\tau$	settling time
$\bar{\cdot}$	baseline value
$\Delta\cdot$	relative variation with respect to baseline value
$\tau_{2\%}$	threshold time value

References

- Leishman, G.J. *Principles of Helicopter Aerodynamics with CD Extra*; Cambridge University Press: Cambridge, UK, 2006.
- Widnall, S. Helicopter Noise due to Blade-Vortex Interaction. *J. Acoust. Soc. Am.* **1971**, *50*, 354–365. [[CrossRef](#)]
- Booth, E.R., Jr. Experimental observations of two-dimensional blade-vortex interaction. *AIAA J.* **1990**, *28*, 1353–1359. [[CrossRef](#)]
- Caradonna, F.; Lautenschlager, J.; Silva, M. An experimental study of rotor-vortex interactions. In Proceedings of the 26th Aerospace Sciences Meeting, Reno, NV, USA, 11–14 January 1988; p. 45.
- Rockwell, D. Vortex-body interactions. *Annu. Rev. Fluid Mech.* **1998**, *30*, 199–229. [[CrossRef](#)]
- Gibertini, G.; Mencarelli, A.; Zanotti, A. Oscillating aerofoil and perpendicular vortex interaction. *Proc. Inst. Mech. Eng. Part G J. Aerosp. Eng.* **2014**, *228*, 846–858. [[CrossRef](#)]
- Droandi, G.; Gibertini, G.; Zanotti, A. Perpendicular blade–vortex-interaction over an oscillating airfoil in light dynamic stall. *J. Fluids Struct.* **2016**, *65*, 472–494. [[CrossRef](#)]
- Chaderjian, N.M. Navier-Stokes simulation of UH-60A rotor/wake interaction using adaptive mesh refinement. In Proceedings of the AHS International Annual Forum & Technology Display, Fort Worth, TX, USA, 9–11 May 2017; number ARC-E-DAA-TN40776.
- Richez, F. Analysis of dynamic stall mechanisms in helicopter rotor environment. *J. Am. Helicopter Soc.* **2018**, *63*, 1–11. [[CrossRef](#)]
- Wilder, M.; Telionis, D. Parallel blade–vortex interaction. *J. Fluids Struct.* **1998**, *12*, 801–838. [[CrossRef](#)]
- Rival, D.; Manejev, R.; Tropea, C. Measurement of parallel blade–vortex interaction at low Reynolds numbers. *Exp. Fluids* **2010**, *49*, 89–99. [[CrossRef](#)]
- Peng, D.; Gregory, J.W. Vortex dynamics during blade-vortex interactions. *Phys. Fluids* **2015**, *27*. [[CrossRef](#)]
- Weingaertner, A.; Tewes, P.; Little, J.C. Parallel vortex body interaction enabled by active flow control. *Exp. Fluids* **2020**, *61*, 137. [[CrossRef](#)]
- Carlson, B.; Ullah, A.H.; Estevadeordal, J. Experimental Investigation of Vortex-Tube Streamwise-Vorticity Characteristics and Interaction Effects with a Finite-Aspect-Ratio Wing. *Fluids* **2020**, *5*, 122. [[CrossRef](#)]
- Barnes, C.J.; Visbal, M.R. Counterclockwise vortical-gust/airfoil interactions at a transitional Reynolds number. *AIAA J.* **2018**, *56*, 2540–2552. [[CrossRef](#)]
- Martínez-Muriel, C.; Flores, O. Analysis of vortical gust impact on airfoils at low Reynolds number. *J. Fluids Struct.* **2020**, *99*, 103138. [[CrossRef](#)]
- Alaminos-Quesada, J.; Fernandez-Feria, R. Effect of the angle of attack on the transient lift during the interaction of a vortex with a flat plate. Potential theory and experimental results. *J. Fluids Struct.* **2017**, *74*, 130–141. [[CrossRef](#)]
- Qian, Y.; Wang, Z.; Gursul, I. Interaction of quasi-two-dimensional vortical gusts with airfoils, unswept and swept wings. *Exp. Fluids* **2022**, *63*, 124. [[CrossRef](#)]
- Seath, D.; Kim, J.M.; Wilson, D. Investigation of the parallel blade-vortex interaction at low speed. *J. Aircr.* **1989**, *26*, 328–333. [[CrossRef](#)]
- Straus, J.; Renzoni, P.; Mayle, R. Airfoil pressure measurements during a blade vortex interaction and a comparison with theory. *AIAA J.* **1990**, *28*, 222–228. [[CrossRef](#)]
- Świrydczuk, J. A visualization study of the interaction of a free vortex with the wake behind an airfoil. *Exp. Fluids* **1990**, *9*, 181–190. [[CrossRef](#)]
- Zanotti, A. Retreating Blade Dynamic Stall. Ph.D. Thesis, Politecnico di Milano, Milano, MI, Italy, 2012.
- Colli, A.; Gibertini, G.; Krishna, P.U.; Marchesi, V.; Zanotti, A. Parallel blade-vortex interaction on pitching airfoil. In Proceedings of the 47th European Rotorcraft Forum (ERF 2021), Glasgow, UK, 7–9 September 2021; pp. 1–13.
- PIVTEC, G. PIVview 2C Version 3.9, User Manual, 2021. Available online: <https://www.pivtec.com/> (accessed on 1 March 2024).
- Raffel, M.; Willert, C.; Wereley, S.; Kompenhans, J. *Particle Image Velocimetry—A Practical Guide*; Springer: New York, NY, USA, 2007.
- Barlow, J.B.; Rae, W.H.; Pope, A. *Low-Speed Wind Tunnel Testing*; John Wiley & Sons: New York, NY, USA, 1999.

27. Goerttler, A.; Braukmann, J.N.; Schwermer, T.; Gardner, A.D.; Raffel, M. Tip-vortex investigation on a rotating and pitching rotor blade. *J. Aircr.* **2018**, *55*, 1792–1804. [[CrossRef](#)]
28. Bandyopadhyay, P.; Balasubramanian, R. Vortex Reynolds number in turbulent boundary layers. *Theor. Comput. Fluid Dyn.* **1995**, *7*, 101–117. [[CrossRef](#)]
29. Ramasamy, M.; Leishman, J.G. A reynolds number-based blade tip vortex model. *J. Am. Helicopter Soc.* **2007**, *52*, 214–223. [[CrossRef](#)]
30. Vatistas, G.H.; Kozel, V.; Mih, W. A simpler model for concentrated vortices. *Exp. Fluids* **1991**, *11*, 73–76. [[CrossRef](#)]
31. Jeong, J.; Hussain, F. On the identification of a vortex. *J. Fluid Mech.* **1995**, *285*, 69–94. [[CrossRef](#)]
32. Wenzinger, C. *Wind-Tunnel Investigation of Ordinary and Split Flaps on Airfoils of Different Profile*; Report (United States. National Advisory Committee for Aeronautics); NACA: Washington, DC, USA, 1935.
33. Loftin Jr, L.K.; Poteat, M.I. *Aerodynamic Characteristics of Several NACA Airfoil Sections at Seven Reynolds Numbers from 0.7×10^6 to 9.0×10^6 (exp 6)*; Technical Report; NACA: Washington, DC, USA, 1948.
34. Althaus, D.; Wortmann, F.X. *Stuttgarter Profilkatalog: Messergebnisse aus dem Laminaerwindkanal des Instituts für Aerodynamik und Gasdynamik der Universität Stuttgart*; Vieweg: Decatur, IL, USA, 1981; Volume 1.
35. Wenzinger, C. *Pressure Distribution Over an N.A.C.A. 23012 Airfoil with an N.A.C.A. 23012 External Airfoil Flap*; Report (United States. National Advisory Committee for Aeronautics); NACA: Washington, DC, USA, 1938.
36. Harvey, J.; Perry, F.J. Flowfield produced by trailing vortices in the vicinity of the ground. *AIAA J.* **1971**, *9*, 1659–1660. [[CrossRef](#)]
37. Walker, J. The boundary layer due to rectilinear vortex. *Proc. R. Soc. Lond. A. Math. Phys. Sci.* **1978**, *359*, 167–188.
38. Doligalski, T.; Smith, C.; Walker, J. Vortex interactions with walls. *Annu. Rev. Fluid Mech.* **1994**, *26*, 573–616. [[CrossRef](#)]

Disclaimer/Publisher’s Note: The statements, opinions and data contained in all publications are solely those of the individual author(s) and contributor(s) and not of MDPI and/or the editor(s). MDPI and/or the editor(s) disclaim responsibility for any injury to people or property resulting from any ideas, methods, instructions or products referred to in the content.